

MICROSCOPY AND MICROANALYSIS



CAMBRIDGE
UNIVERSITY PRESS

Comparing the consistency of atom probe tomography measurements of small-scale segregation and clustering between the LEAP 3000 and LEAP 5000 instruments

Journal:	<i>Microscopy and Microanalysis</i>
Manuscript ID	MAM-APTM16-16-130.R1
Manuscript Type:	APT&M2016 Special Issue
Date Submitted by the Author:	07-Feb-2017
Complete List of Authors:	Martin, Tomas; University of Oxford, Department of Materials London, Andrew; University of Oxford, Department of Materials Jenkins, Benjamin; University of Oxford, Department of Materials Hopkin, Sarah; University of Oxford, Department of Materials Douglas, James; University of Oxford, Department of Materials Styman, Paul; National Nuclear Laboratory Bagot, Paul; University of Oxford, Department of Materials Moody, Michael; University of Oxford, Department of Materials
Keywords:	atom probe tomography, clustering, small-scale segregation, detector efficiency, Steel

SCHOLARONE™
Manuscripts

Comparing the consistency of atom probe tomography measurements of small-scale segregation and clustering between the LEAP 3000 and LEAP 5000 instruments

Tomas L. Martin^{*1}, Andrew J. London¹, Benjamin Jenkins¹, Sarah E. Hopkin¹, James O. Douglas¹, Paul D. Styman², Paul A. J. Bagot¹ and Michael P. Moody¹

¹ Department of Materials, University of Oxford, Parks Road, Oxford, United Kingdom OX1 3PH

² National Nuclear Laboratory, Building D5, Culham Science Centre, Abingdon, Oxfordshire, United Kingdom OX14 3DB

*Corresponding author: tomas.martin@materials.ox.ac.uk

Abstract

The local electrode atom probe (LEAP) has become the primary instrument used for atom probe tomography measurements. Recent advances in detector and laser design, together with updated hit detection algorithms, have been incorporated into the latest LEAP 5000 instrument, but the implications of these changes on measurements, particularly the size and chemistry of small clusters and elemental segregations, have not been explored. In this study, we compare datasets from a variety of materials with small-scale chemical heterogeneity using both a LEAP 3000 instrument with 37% detector efficiency and a 532nm green laser and a new LEAP 5000 instrument with a manufacturer estimated increase to 52% detector efficiency, and a 355nm UV laser. In general, it was found that the number of atoms within small clusters or surface segregation increased in the LEAP 5000, as would be expected by the reported increase in detector efficiency from the LEAP 3000 architecture, but subtle differences in chemistry were observed which are attributed to changes in the way multiple hit detection is calculated using the LEAP 5000.

1. Introduction

Atom probe tomography (APT) evolved from field ion microscopy, beginning with the one-dimensional atom probe in the 1960s (Muller *et al.* 1968) and the 10cm Atom Probe in the 1970s (Panitz, 1973) and eventually moving to genuinely three dimensional analysis in the late 1980s (Cerezo *et al.* 1988); (Blavette *et al.* 1989). ~~Whilst~~ While these developments allowed the atomic-scale structure of materials to be probed in three-dimensions, the analysis volumes incorporated by the measurements were limited. The development of the local electrode atom probe (LEAP) in the late 1990s, (Kelly *et al.* 1996) ~~and~~ (Kelly *et al.* 2000), represented a significant improvement in the rate at which the specimen could be sampled. Later, the use of silicon microtip coupons, in combination with new specimen preparation methods using focused ion beam (FIB) (Lawrence *et al.* 2007) and laser-pulsing capability (Bunton *et al.* 2007), opened up APT to many new materials and areas of study.

Currently, the Cameca LEAP series is by far the most widely used atom probe instrument, with over 85 installed worldwide by early 2016. These instruments are used by many research institutions to study applications including identifying the chemistry of small phase changes in metals (Steiner *et al.* 2016), characterising the boundaries of corrosion surfaces (Pedrazzini *et al.* 2016) and even individual cracks (Meisnar *et al.* 2015), whole semiconductor transistors (Inoue *et al.* 2009), catalysis (Li *et al.* 2012), and more recently moving outside of traditional materials science applications and into fields such as geoscience (Valley *et al.* 2014) and biological materials (Gordon *et al.* 2012).

The first widely commercially available instrument in this series was the LEAP 3000. Available in a reflectron-equipped configuration with a detection efficiency around 37% and a straight flight path configuration with a detection efficiency of ~57% (Moody *et al.* 2011), the LEAP 3000 could be fitted with a green 532nm laser and used up to frequencies of 250kHz (Larson *et al.* 2013). In 2011 the LEAP 4000 was released, with essentially the same three-chamber set up and detector configuration as the LEAP 3000, but changes in laser design and the addition of a stability-improving air table to the frame. This allowed a change in laser wavelength to a UV 355nm laser with a smaller spot size, which has been shown to reduce thermal tails in the mass spectrum and improve yield in many brittle or non-conductive materials (Larson *et al.* 2013).

In 2015, the latest generation of atom probe instrument, the LEAP 5000, was announced. This instrument incorporates both the UV laser configuration of the LEAP 4000 as well as a completely new position-sensitive detector setup. The most significant improvements in the ion detection system are the change in microchannel plate (MCP) geometry and an updated hit detection algorithm to better identify multiple hit events. The LEAP 5000 design replaces the cylindrical channels in the MCP found in the LEAP 3000 and 4000 with a newer design where the openings of each channel are widened into a conical shape, reducing the deadspace between channels where impacting ions do not create a signal. Consequently, this increases the detection efficiency of the instrument to a reported ~52% for the reflectron equipped model and ~81% for the straight flight path instrument (Prosa *et al.* 2014).

In early 2016, the University of Oxford acquired a new LEAP 5000XR, to complement the LEAP 3000X HR used at the university since 2007. The presence of both machines in the same research lab offers the opportunity to make comparisons between the two instruments on a wide variety of material systems. There have been a number of studies comparing the effect of the laser wavelength on atom probe measurements (Amouyal & Seidman, 2012); (Santanagolan *et al.* 2015), and so this study will not explore the effect of laser energy other than to attempt to use equivalent laser powers when comparing results in laser mode between the two instruments. Instead, this study will use a variety of materials with small-scale chemical segregation to explore the effect of the change in detector geometry and hit detection on the size and chemistry of small clusters and surface segregation.

There has been work in the literature to quantify the effect of dead time on the efficiency of microchannel and delay line detectors, and Jagutzki *et al.* showed that the use of a third delay line results in better readout of multihit events, both by reducing ambiguity for simultaneous events, but also by reducing the size of the dead region on the detector after a hit, increasing the chance that a subsequent hit will be detected (Jagutzki *et al.* 2002). Similarly, the work of Meisenkothen *et al.* explored the effects of detector dead-time on boron, one of the elements most prone to field evaporating preferentially in multiples. They showed that the dead-time surrounding the first hit in a pulse contributes most to the under-reporting of boron (Meisenkothen *et al.* 2015). In this study, however, the focus was on the practical effects of the change in detector on specimens for materials science projects rather than model systems, to

~~aid allow~~ users of LEAP instruments to be aware of the effects switching between the instruments might have on their data.

The materials chosen for this project present a variety of different microstructures and chemistries in order to identify the influence of the change in detector design between the two instruments. Firstly, to characterise the impact of detector efficiency on cluster detection and analysis, two steels containing nanometre-scale clustering were analysed. The first steel was an SG Steel with small-scale clustering containing only metallic species. The second was an oxide-dispersed strengthened (ODS) steel, where the clusters contained large quantities of oxygen, to determine whether ~~the presence of~~ oxide species behave differently than metallic clusters with a change in detection efficiency.

Comment [JM1]: define

The third steel contained carbide precipitates, as the composition observed from carbon containing materials ~~such as carbon~~ prone to evaporation in multiple ions is known to be affected by changes in detection efficiency (Thuvander, *et al.* 2013, Rolander and Andren, 1989, Kinno *et al.* 2012, Cerezo, Smith and Waugh, 1984). Lastly, a silicon sample containing small quantities of implanted phosphorus was studied, to compare the effects of the change in detector on the observation of low levels of non-clustered impurities.

2. Materials and Methods

Four materials with microstructural heterogeneities on a scale appropriate to be sampled by APT analysis were used in this study: three steels, incorporating metallic, oxide and carbide

precipitates, respectively, and a phosphorus-implanted silicon material with low concentrations of the implanted dopants close to the surface.

The first steel sample was a Rolls Royce SG model alloy steel used in nuclear reactor pressure vessels, with a composition of 1.52% Mn, 0.81% Si, 0.43% Cu, 0.29% Ni, 0.28% Mo and 0.24% C (all wt.%). Prior to ageing, all specimen blocks underwent a standard post weld heat treatment of annealing at 920 ± 20 °C for 6 hrs followed by a water quench, then tempering at 600 ± 15 °C and stress relief at 650 ± 15 °C for 42 hrs and 6 hrs respectively followed by slow cooling (≤ 50 °C hr⁻¹) after each treatment stage. Samples were aged in sealed quartz tubes under Ar atmosphere or vacuum to limit the effects of oxidation and were water quenched upon removal from the furnace.

The second material was an oxide-dispersion-strengthened (ODS) steel with nominal composition Fe-0.3wt%Y₂O₃, as well as trace amounts of W, Cr and Ti. The material was produced by mechanical alloying followed by hot-isostatic pressing, as described by Robertson *et al.* (Robertson et al.2012)

The third material and final alloy sample was an M50 bearing steel prepared at the Cambridge SKF University Technology Centre, containing 4.38% Cr, 3.84% C, 2.40% Mo, 1.05% V and lower levels of Mn, Si and Al (all at.%). A VIM-VAR casting process was followed by hot-rolling and soft-annealing for two hours at 880°C. The ingot was then cooled to 600°C over 11 hours. A five-minute austenisation in a vacuum furnace at 1105°C was followed by quenching to room

temperature. Three tempering cycles were performed at 545°C for two hours each with two hour cryogenic treatments between the tempering cycles.

For each of the three steels, the bulk material was cut into 25x0.5x0.5 mm matchsticks using a Buehler Isomet 5000 diamond wafering saw and needle specimens of each steel were produced using a two-stage electropolishing process, using standard preparation methods (Gault *et al.* 2012). Each matchstick was first electropolished using 25% perchloric acid (60%) in acetic acid, using voltages between 5-16V DC to control etching speed, until the matchstick split into two needle-shaped specimens. These specimens were then more finely polished under a microscope using 2% perchloric acid (60%) in 2-butoxy-ethanol and voltages of 8-15V DC, to produce needles with an end radius of ~100nm.

The LEAP 5000 samples of the SG steel were prepared using standard FIB lift-out procedures (Lawrence *et al.* 2007) ~~due to because the~~ quantity of heat-treated material available ~~being was~~ insufficient for electropolishing. Tungsten was deposited onto the region selected for lift-out via electron beam using a Gas Injection System for two minutes. This was followed by a further two minutes of tungsten deposition using the ion beam at 30kV, to provide additional protection from Ga damage during milling.

The phosphorus implanted silicon samples used the standard reactive ion etched silicon flat top micro post coupons used for LEAP analysis. The coupons were HF dipped and the micro posts were implanted directly with 14keV phosphorus ions, with the fluence calculated to give 0.2

at.% peak concentration at a depth of ~22nm. Following implantation the sample was HF dipped again prior to capping with Ni (LEAP 3000 sample) or directly coated in Co without an HF dip (LEAP 5000 sample), in both cases using a thermal evaporator with 99.99% pure metal sources in an initial vacuum of $\sim 10^{-6}$ Torr, before tungsten protection in the FIB instrument as for the RPV specimens. Micro posts were then polished into a sharp tip using a Zeiss NVision Focused Ion Beam instrument. These capped micro posts were annular milled at 30kV until the capping layer/silicon interface was approximately 200nm from the top of the specimen, and then polished using a 2kV ion beam to remove all the tungsten cap and all but ~15nm of the Ni or Co cap, finishing with a final tip radius below 100nm.

All four materials were analysed in both the LEAP 3000 and LEAP 5000. Although some of the older LEAP 3000 instruments have a two anode delay line detector, the Oxford instrument has the later three anode delay line detector, making comparisons between the 3000 and 5000 more straightforward. Settings were kept as similar as possible for ease of comparison, bearing in mind that due to the smaller laser spot size on the LEAP 5000, the laser energy of the UV laser on the LEAP 5000 is approximately one order of magnitude smaller to produce evaporation conditions that are comparable to that of the green laser on the LEAP 3000. Table 1 summarises the specimen temperature, pulse energy/fraction and frequency used for each material on both instruments. For the ODS steel, the pulse energy was varied between 0.2-0.6nJ on the LEAP 3000 and from 0.01 -0.16nJ on the LEAP 5000 to observe the effect of laser energy on cluster composition.

The reported results are the average from multiple specimen tips, so that the data is not unduly affected by compositional heterogeneity. In the case of the RPV steel SG, 4 datasets were obtained using the LEAP 3000 and 5 datasets were obtained using the LEAP 5000. The carbide and ODS steel cluster data was also obtained over several datasets. Whilst the data presented for the phosphorus implanted silicon was only from one dataset, it was compared to other repeated data and the same results were observed – only one profile from each machine is shown, as aligning the exact position of the start of the implantation profile results in averaging that smooths out the signal. It should be noted that due to sample yield the number of atoms collected for each instrument varied, and as such the total number of clusters detected is not directly comparable for each material, but as the statistics of all clusters are being studied, this should not affect the results of this study.

Datasets were analysed using the commercial software IVAS, version 3.6.12. Clusters in the SG and ODS steels were identified in the data using the method of maximum separation distance of “solute” atoms (Hyde *et al.* 2011). Ions within a maximum separation (D_{\max}) of each other are considered clustered. The D_{\max} parameter was kept the same between datasets from both instruments, but the N_{\min} parameter (the minimum number of ions in a cluster) was varied to suit the number of clusters observed. In the bearing steel and the silicon sample, isoconcentration surfaces were used to identify the carbide precipitates and capping layer respectively.

Where appropriate, the cumulative distribution of clusters $F(t)$ was compared between the two instruments using the empirical distribution function:

$$\hat{F}_n(t) = \frac{\text{number of elements in the sample } \leq t}{n} = \frac{1}{n} \sum_{i=1}^n 1_{x_i \leq t}$$

Where 1_z is the indicator of event z . Comparing the two datasets in this manner allows small changes in size distribution to be more easily distinguished. Assuming a LEAP 3000 efficiency of 37% and a LEAP 5000 efficiency of 52%, we should expect that multiplying the LEAP 3000 cumulative distribution by the ratio between the two efficiencies (~ 1.405) should give the same distribution as observed in the LEAP 5000 data, providing sufficient statistics are obtained for both.

3. Results

Figure 1 shows example atom maps for the four types of materials used in this study. Three were steels with different types of cluster – metallic, oxide and carbide, whilst the final material is an implanted semiconductor with low levels of impurity at a small region near the surface. In each case, small features were chosen to see if the change in detector efficiency resulted in the expected increase in atom count in the features, as well as comparing the effect on other aspects of the data such as cluster composition. Cluster size was defined as the number of solute ions in the cluster, except in cases where the cluster radius was used, as defined in nm.

3.1 Copper clusters in an SG steel (voltage mode)

The simplest comparison is between two metals with small-scale clustering in voltage mode, where the effects of laser wavelength cannot affect the measurements. In the reactor pressure vessels of nuclear reactors, even small cluster formation during operation can be detrimental to the lifetime of the reactor, particularly if the clusters are of an element with a larger atomic radius than the matrix such as Cu (Styman *et al.* 2012). This study selected one such material, where nanometre-scale Cu precipitates were known to occur after long-term ageing. These clusters can often be very small, and identifying them from the matrix at the early stages of formation can be challenging; it is hoped that the higher efficiency detector will potentially aid in the observation of early-stage clustering.

Figure 2(a) shows the size distribution of the Cu clusters across four datasets obtained on the LEAP 3000 (in black) to five datasets obtained on the LEAP 5000 (in blue), whilst Figure 2(b) shows the empirical distribution function for the same data. The latter more obviously shows the difference between the two distributions. There are a similar number of large-scale clusters (above ~5000 atoms), but more clusters are observed at low atom counts in the LEAP 5000, particularly for clusters less than 1000 atoms. The median count of solute atoms was 218 atoms in the LEAP 3000, but only 129 atoms in the LEAP 5000, despite the median cluster radius remaining essentially unchanged, at 1.17nm for the LEAP 3000 data and 1.13nm for the LEAP 5000 data. A possible interpretation of this result is that the higher efficiency of the LEAP 5000 is enabling more of the clusters, which contain fewer atoms, present in the material to be observed, as expected. Since some of the clusters were not being detected previously in the

LEAP 3000 datasets, it is hard to estimate the detector efficiency increase based on comparing the two distributions.

Figure 3 compares the chemistry of all 119 clusters in the LEAP 3000 data and 85 clusters in the LEAP 5000 data. Over four LEAP 3000 datasets, 45 million atoms of data was obtained, compared to five LEAP 5000 datasets totalling just over 30 million atoms, so although the total number of clusters should not be compared directly, sufficient data was obtained to compare the statistics between the two instruments. While ~~the~~ scatter in the composition plots in Figure 3(a) and (b) is high, there is a trend for the average Fe content to be higher in the LEAP 3000 data than in the LEAP 5000 data, by approximately 3 at.%, with a corresponding drop in Cu and Mn solute. When the Fe content is normalised to the reduced cluster radius, as in Figure 3(c), this trend, although slight, remains. The measured Fe concentration in the clusters is likely incorporating a significant contribution from the surrounding matrix as a result of magnification effects due to the difference in evaporation field between the Cu and Fe (Larson *et al.* 2013); (Gault *et al.* 2012). One possible explanation is that the difference highlighted in Fig. 3 results from the change in hit detection algorithm with respect to multiple hit events. Fe-Fe pairs account for 99% of the multiple ions detected, therefore any improvement in the recognition of multiple hits will predominantly increase the detection of Fe. ~~Therefore-Thus,~~ if the algorithm improves the discrimination of individual ions within multiple hit events, it could explain the increased Fe content measured in these clusters.

3.2 Yttrium Oxide particles in an oxide-dispersed steel (laser mode)

Oxide particles are another form of clustering in steels that can be important at the scale where detection efficiency changes could be important to the analysis. For the purpose of this study, it is also a material where the size of particles in an ODS steel is more uniform than for the SG steel, as the particles are dispersed mechanically rather than grown during ageing.

Figure 4 compares the distribution of particles in two datasets. The LEAP 3000 dataset contained 791 clusters, whilst the LEAP 5000 dataset contained 495 clusters, with a median solute (Y and YO) count of 101 and 127 atoms per cluster, respectively. The difference in absolute numbers of clusters is primarily because 70 million atoms of data were obtained on the LEAP 3000 compared to 48 million atoms on the LEAP 5000, but this should not affect the comparison between individual cluster behaviour on the two instruments. In the size distribution plot in Figure 4(a), we observe that the curve is shifted lower for the LEAP 3000, with a higher number of smaller clusters between 0 and 300 atoms, and a slightly decreased tail between 300 and 600 atoms, when compared to the LEAP 5000 distribution. The empirical distribution function in Figure 4(b) makes this easier to observe, showing a clear shift in the distributions for clusters with between ~100-500 solute atoms. Comparing the actual values of the two curves, however, the clusters in the LEAP 5000 contain only about 1.2 times the number of atoms as the LEAP 3000 data, rather than the 1.4 times expected by the change in detector efficiency, and implying an effective LEAP 5000 detector efficiency of 44%. This discrepancy is likely due to the fact that, in the LEAP 3000 data, the maximum separation method has difficulty in fully distinguishing between the smallest clusters, visual inspection of the datasets shows that in a number of cases clusters are identified by the algorithm that

appear to be two or more clusters joined together. This will artificially increase the measured size of the LEAP 3000 clusters, resulting in a smaller difference compared to the LEAP 5000 data, where more individual clusters are identified accurately without merging.

Figure 5 explores the chemistry of the ODS particles in the two machines, this time by considering data from a variety of laser energies. The composition of the particles considering only the solute elements with increasing laser energy is compared between the two instruments in Figure 5(a) for the LEAP 3000 and Figure 5(b) for the LEAP 5000. The quantity of lighter elements such as O and N decreases with increasing laser energy in both instruments, and it can be seen that roughly comparable compositions can be obtained by using a UV laser energy approximately ten times smaller than that used for the 532nm green laser in the LEAP 3000.

Figure 5(c) compares the Fe content observed within these particles normalised to cluster radius. It can be observed that the distribution is shifted between the two instruments, and that more Fe is observed for an equivalent particle in the LEAP 5000 data. As with the Cu clusters in the SG steel, the included Fe is at least in part an aberration of magnification effects due to the change of evaporation field between the YO particles and the matrix, but there could also be a contribution from the need for a different erosion step during the cluster analysis.

3.3 Carbides in a bearing steel (laser mode)

Another ~~form-kind~~ of small-scale precipitate found in many steels are the various forms of carbides. For this study a high-carbon bearing steel was chosen due to the large number of carbides present in a single atom probe dataset. A selection of comparable M_2C carbide particles were selected from datasets from both the LEAP 3000 and LEAP 5000. These carbides were analysed using an isoconcentration surface of 13 at.% C. The larger VC and cementite carbide particles were excluded based on their chemistry, as were any particles not fully enclosed in the dataset, and those below 6nm^3 in size, which could be attributed to random fluctuations in the analysis. The selection criteria resulted in 8 similar sized carbides in each dataset.

Table 2 compares the ion count and composition of the selected carbides. The eight carbides in each of the two datasets averaged the same volume, but the LEAP 5000 data contained more ions, as would be expected. Based on the 170 average ions in the LEAP 3000 and a LEAP 3000 detector efficiency of 37%, this implies a LEAP 5000 efficiency of 53%, very close to the expected value.

As with the other steel materials analysed in this study, the average measured chemistry of the carbides changes between the two instruments. The average carbon concentration inside the selected carbides decreased from 35.2% in the LEAP 3000 to 26.1 at.% in the LEAP 5000, with a corresponding increase in iron content from 20.0% in the LEAP 3000 to 27.2% in the LEAP 5000. Unlike the other particles in this study, this Fe is expected to be part of the actual carbide composition. Other elements did not change significantly. It is also seen that the percentage of

carbon atoms being labelled as multiple hit events increases from 74.3% of carbide C atoms in the LEAP 3000 to 85.9% in the LEAP 5000 data, despite the overall multiple count of all the atoms in the datasets remaining at 6% in both instruments.

-Thuvander *et al.* showed that by reducing the efficiency of a LEAP 3000 with the introduction of a grid behind the electrode, more carbon was detected in a tungsten carbide specimen (Thuvander, 2013). This implies that as the detector efficiency increases, the overall efficiency of the detector to observe multiple-hit events, such as C ions, increases less than for single ion events. It appears that the changes in the algorithm for multiple hit detection are still not sufficient to prevent some losses in C content due to C ions ~~impacting-hitting~~ the detector at a similar position, within the dead time of the delay line detector. Whilst this effect can be reduced by altering the analysis parameters (Marceau, 2013), it remains the case that as the detector efficiency of the current APT detector technology improves, the multiple hit performance will become a challenge to obtaining accurate compositions of materials containing elements with tendency to evaporate in multiples (Kinno *et al.* 2013).

3.4 Implanted phosphorus at the surface of silicon (laser mode)

It is not only metals where small-scale features can be affected by the change in detector configuration. Phosphorus centres in silicon are a promising possible qubit for use in quantum computing (Kane, 1998), but there are extreme spatial constraints in the placement of individual atoms. Phosphorus atom placement using Scanning Tunnelling Microscopy allows precise control of the locale of single atoms and has been used in extremely promising initial

studies (Fueschsle, 2012), but it is slow, expensive and unlikely to be easily scaled up to the industrial levels required for commercial quantum computing arrays. Ion implantation is a well understood industrial process commonly used in fabrication of integrated semiconductor electronics and the implantation and detection of single phosphorus ions within designated nanoscale volumes has already been demonstrated (Donkelaar, 2015).

APT investigations of silicon implanted with 14 keV phosphorus ions with peak concentration of 0.2 at.% have been carried out using the LEAP 3000 (Douglas, 2016) and LEAP 5000. An increase in detector efficiency could improve the ultimate detection limit of phosphorus in silicon for this application and allow more accurate characterisation of low concentration diffusion and implantation profiles in general.

Comparing the behaviour of 0.2 at.% phosphorus implantation in silicon between the two LEAP instruments is complicated by the increase in the number of P-containing complex ions in the mass spectrum of the LEAP 5000 (likely due to on the change in laser wavelength), as well as overlaps with the Ni/Co metal used to cap the silicon.

To minimise the effect of any surface migration, both datasets were cropped into 30x30x100nm regions of interest from the centre of the dataset, as shown in Figure 6 (a) and (c). Figure 6 (b) and (d) show the phosphorus profile from the end of the capping layer signal into the silicon in these two regions, with the large increase on the right-hand side at ~0nm indicating the start of the capping layer. In both LEAP instruments, the concentration profile in at.% shown in

Figure 6(b) match well, with a peak of approximately 0.2 at.% around 15nm below the surface, a little shallower than the 22nm predicted by simulation (Donkelaar, 2015)^{Error! Bookmark not defined.}. If, instead of the concentration, the absolute number of phosphorus atoms is plotted, as shown in Figure 6(d), the difference between the two instruments becomes clearer – with a high peak value of phosphorus in the LEAP 5000.

Although the quantity of phosphorus atoms observed is close to that expected for the LEAP 5000 efficiency, it comes with some caveats. Due to the very low numbers of atoms involved in this implanted layer, even very small changes in the number of phosphorus atoms included in the calculation can make a big difference in the expected efficiency. Varying the binning size of the concentration profile or the value of the isoconcentration surface used to define the end of the capping layer, even slightly, can dramatically change the number of phosphorus atoms observed. Varying the parameter selection from a bin size of 0.5-2nm and the isoconcentration surface from 3-5% Ni or Co has a large impact on the number of reported phosphorus ions. Particularly the isoconcentration surface value used to determine the point at which the Ni or Co capping layer ends and the implanted silicon begins. Based on the number of P ions detected using the extremes of these two parameters, the calculated efficiency of the LEAP 5000 could range anywhere from 41.7% to 67.6%.

The principle reason for such uncertainty is that the bins closest to the capping layer interface contribute both from P ions and also from overlaps in the $\text{Ni}^{2+}/\text{P}^+$ (at 31 Da) or Co/SiP (at 59 and 29.5 Da). If the P ion count is summed across a 40nm depth profile region starting directly

below the interface, the efficiency in the LEAP 5000 is overestimated due to additional counts from overlapped Co ions. Conversely, for profiles starting more than 7.5nm below the interface, the LEAP 5000 efficiency is underestimated, as we start to lose actual P ions in the datasets. Profiles beginning 6.5 -5.5 nm below the interface, give an efficiency of 51.5-51.8 %, close to the expected value. In this way, if the efficiencies of both detectors are accurate, they allow the use of the ratio between the two measurements to calibrate the accuracy of measured data.

4. Discussion

4.1 Comparing cluster and carbide size with increased detection efficiency

The implications of this study suggest that the efficiency gain due to the change in microchannel plate design in the LEAP 5000 generation is close to that expected by an increase from 37% to 52%, subject to caveats regarding parameter choice. Since the smaller Cu clusters in the SG steel were not detected in the LEAP 3000, due to its reduced detection efficiency, the decrease in cluster size in the LEAP 5000 data is due to the increased sensitivity to these small features, making comparison of the cluster size between the two detectors difficult. Similarly, the propensity of the maximum separation method to merge small clusters together in the LEAP 3000 analysis of the ODS steel results in a lower than expected increase in cluster size in the LEAP 5000 – it is possible that improvements in cluster-finding algorithms may make such comparisons more accurate.

In the case of the carbide-containing steel and phosphorus-implanted silicon, the increase in atoms in the features increased roughly in line with the expected efficiency gain, although in

both cases the choices of analysis parameters, especially the isoconcentration surface value used to define the edge of the carbide and the capping layer respectively, make a big difference to this calculation, ~~so~~. Hence, it is difficult to ascribe too much confidence to this calculation – analysis parameter choice remains vital to accuracy.

The third case, where dramatically more carbon was observed in M_2C carbides of the same size in the LEAP 3000, is slightly different. The increase in detector efficiency does appear to be resulting in a reduction in carbon content, as a result of increased loss of data from carbon multiple hit events, despite the change in hit finding algorithm on the LEAP 5000. It will remain the case that for increased detector efficiency, there will be decreased ability to distinguish multiple ion events (Thuvander, 2013), and as a result the actual concentration of C may be underestimated further on higher efficiency instruments.

The phosphorus-implanted silicon material, perhaps even more so than the other materials, shows the importance of parameter selection during analysis of atom probe data. Varying the parameters of the isoconcentration profile used to define the start of the analysed region can dramatically impact the number of phosphorus ions observed, resulting in an effective efficiency of the LEAP 5000 anywhere from 41% to 67%.

4.2 Changes in stoichiometry between LEAP instruments

Whilst the change in detected atoms within these features either corresponds well to the detector change or can be explained, chemistry variations in the three steel samples are harder to account for. In all three cases, the composition was observed to differ between the LEAP 3000 and LEAP 5000. In the Cu clusters, more Fe was included from the matrix in the LEAP 3000, whilst in the ODS steel, the reverse was observed, with more Fe content in the LEAP 5000 clusters.

In the SG steel, the higher percentage of Fe observed in the LEAP 3000 data is slight, but present. The ODS particles also saw a change in average Fe content between the two machines, although in this case the effect was reversed, with more Fe in the LEAP 5000 data. There are several possible reasons for this effect – it may be that the hit finding algorithm is also playing a part here – the sample is mostly Fe, so if the rate of detected multiple ions increasing, the Fe concentration would be more effected by a general increase in multiple ions. It could also be that the increased number of atoms detected in the LEAP 5000 requires a change in cluster finding parameters – as the D_{\max} and erosion parameters were kept the same for both instruments, it is possible that this has affected the behaviour of Fe included at the edge of the clusters. The reason behind the reversed direction of the increased Fe content between the two materials is intriguing. If the nature of the matrix aberration was different – i.e. that one was a high field precipitate where the Fe inclusion was due to spreading of the higher field precipitate across the matrix, and the other was a low field precipitate where the Fe was included mainly as a magnification effect – it may be that the change in detector efficiency results in a different effect on the two aberration types.

Whilst the improvements in detector efficiency and hit-finding algorithms are to be welcomed in the LEAP 5000 instrument, it will remain the case that careful data analysis is often the most important factor in the accurate use of APT. It is important that the differences between measurements taken on both instruments is understood so that experiments using different generations of APT instruments can be compared.

5. Conclusion

Atom probe tomography datasets from four materials were compared using a LEAP 3000X HR with a 37% detection efficiency and a 532nm green laser, and a LEAP 5000XR with 52% detection efficiency and a 355nm UV laser. Small segregations of clusters or impurity elements were compared to determine the effect of the change in instrument on the size and chemistry of these small-scale features. When comparing the ion count of the segregated elements in a carbide-containing steel and phosphorus-implanted silicon, the LEAP 5000 showed an increase in counts roughly equal to the expected change in detector efficiency, although it was also shown that the choice of isoconcentration surface used to perform this analysis can dramatically impact this calculation. The size distribution of Cu clusters in an SG steel was harder to directly compare, due to the detection of additional small particles using the LEAP 5000 that were previously undetectable in the LEAP 3000, whilst in the case of YO particles in an ODS steel, the difference was smaller than expected, likely due to merging of small particles during the cluster analysis.

The detector change appeared to give the expected increase in detected atoms, but the effect of the change in instrument on composition was less clear-cut. In the case of the three steel samples, the composition of Fe and/or C in the particles varied between the two instruments. In the carbides of the bearing steel, significantly lower carbon content is present in the LEAP 5000 data, which we ascribe to the reduced ability of the detector to distinguish multiple hit events at the higher efficiency, despite the change in hit detection algorithm in the newer instrument. In the SG and ODS steel, the level of iron included from the matrix into the particle composition varied between the two instruments, although the direction of this effect differed between the two materials, with more Fe in the Cu clusters in the LEAP 3000, but more Fe in the ODS particles in the LEAP 5000 data. This effect is more challenging to explain, but the hit finding algorithm could also play a role, as could variations in the evaporation field between cluster and matrix, or the parameters chosen for the cluster search. In general, the reliability of results between the two instruments is consistent, but the study highlights that choice of analysis parameters when making isoconcentration surfaces or cluster searches can often be more significant to the size of the observed feature than the change in detector geometry.

Figure Captions

Figure 1: Atom maps for the materials used during this study. (a) Cu clusters in a thermally aged Reactor Pressure Vessel (RPV) steel, (b) Yttrium Oxide clusters in an Oxide Dispersion Strengthened (ODS) steel, (c) carbides in a bearing steel and (d) phosphorus at the surface of implanted silicon. All atom maps shown were analysed using the LEAP 3000.

Figure 2: (a) Comparison of the size distribution of Cu clusters in an RPV steel analysed on the LEAP 3000 (black) and LEAP 5000, (blue). (b) Empirical cumulative distribution function comparing the two distributions.

Figure 3: Compositions of the Cu clusters in (a) four LEAP 3000 datasets and (b) five LEAP 5000 datasets, against cluster size, as defined by the number of ranged ions. The Fe content averaged 53-at.% in the LEAP 3000 and 50-at.% in the LEAP 5000. (c) shows the Fe content as a function of cluster radius for the two instruments.

Figure 4: (a) Size distribution of YO particles in an ODS steel analysed using the LEAP 3000 (black) and LEAP 5000 (blue). (b) shows the empirical cumulative distribution function for the same data.

Figure 5: (a) Change in YO particle chemistry with increasing laser energy on the LEAP 3000 (b) change in YO particle chemistry with laser energy on the LEAP 5000, (c) the relationship between cluster size and Fe content included from the matrix in the oxide particles, with black representing data from the LEAP 3000 and blue representing data from the LEAP 5000.

Figure 6: (a) 30x30x100nm region of interest of a phosphorus-implanted silicon sample with nickel cap analysed using the LEAP 3000. (b) Comparison of the phosphorus concentration profile at the surface of both ion-implanted silicon materials. (c) 30x30x100nm region of interest of a phosphorus-implanted silicon sample with cobalt cap analysed using the LEAP 5000. (d) Ion counts of phosphorus across the same region shown in (b).

Table Captions

Table 1: Summary of APT analysis conditions used for each of the four materials used in this study, for both the LEAP 3000 and LEAP 5000 instruments.

Table 2: Comparison of the size, number density and composition of selected M_2C carbides analysed from a bearing steel in the LEAP 3000 and LEAP 5000 instruments.

References

- AMOUYAL, Y. & SEIDMAN, D.N. (2012). Atom-Probe Tomography of Nickel-Based Superalloys with Green or Ultraviolet Lasers: a Comparative Study, *Microscopy and Microanalysis*, 18(5), pp. 971-981
- BOSTEL, A., BLAVETTE, D., MENAND, A. & SARRAU, J.M. (1989) Toward a tomographic atom-probe. *Colloq. Phys.* 50(C8), pp. 501-506
- BUNTON, J.H., OLSEN, J.D., LENZ, D.R. & KELLY, T.F. (2007). Advances in pulsed-laser atom probe: instrument and specimen design for optimum performance. *Microsc. Microanal.* 13, pp.418-427
- CEREZO, A., GODFREY, T.J. & SMITH, G.D.W. (1988). Application of a position-sensitive detector to atom probe microanalysis. *Rev. Sci. Instrum.* 59(6), pp. 862-866
- CEREZO, A., SMITH, G.D.W. & WAUGH, A.R. (1984). The FIM100 – Performance of a commercial atom probe system. *J. Phys. Colloques.* 45, C9-329-C9-335
- DONKELAAR, J.V., YANG, C., ALVES, A.D.C., MCCALLUM, J.C., HOUGAARD, C., JOHNSON, B.C., HUDSON, F.E., DZURAK, A.S., MORELLO, A. & SPEMANN, D. (2015). Single atom devices by ion

implantation, *J. Phys.: Condens. Matter* 27 154204

DOUGLAS, J.O., BAGOT, P.A.J., JOHNSON, B.C., JAMIESON, D.N. & MOODY, M.P. (2016).

Optimisation of sample preparation and analysis conditions for atom probe tomography characterisation of low concentration surface species, *Journal of Semiconductor Science and Technology*, In Press

FUECHSLE, M., MIWA, J.A., MAHAPATRA, S., RYU, H., LEE, S., WARSCHKOW, O., HOLLENBERG, L.C.L., KLIMECK, G. & SIMMONS, M.Y. (2012). A single-atom transistor, *Nat Nano*, 7(4), pp. 242-246

GAULT, B., MOODY, M.P., CAIRNEY, J.M. & RINGER, S.P. (2012). *Atom Probe Microscopy*, Springer Series in Materials Science, 160, Verlag New York: Springer

GORDON, L.M., TRAN, L. & JOESTER, D. (2012). Atom Probe Tomography of Apatites and Bone-Type Mineralized Tissues, *ACS Nano* 6(12), pp. 10667-10675

HYDE, J.M., MARQUIS, E.A., WILFORD, K.B. & WILLIAMS, T.J. (2011). A sensitivity analysis of the maximum separation method for the characterisation of solute clusters, *Ultramicroscopy*, 11(6), pp. 440-447

- INOUE, K., YANO, A., NISHIDA, A., TAKAMIZAWA, H., TSUNOMURA, T., NAGAI, Y. & HASEGAWA, M. (2009). Dopant distributions in n-MOSFET structure observed by atom probe tomography, *Ultramicroscopy*, 109(12), pp. 1479-1484
- JAGUTZKI, O., CEREZO, A., CZASCH, A., DÖRNER, R., HATTAß, M., HUANG, M., MERGEL, V., SPILLMANN, U., ULLMANN-PFLEGER, K., WEBER, T., SCHMIDT-BÖCKING, H. & SMITH, G.D.W. (2002). Multiple hit readout of a microchannel plate detector with a three-layer delay-line anode, *IEEE Transactions on Nuclear Science*, 49, pp. 2477-2483
- KANE, B.E. (1998). A silicon-based nuclear spin quantum computer, *Nature* 393 pp. 133–137
- KELLY, T.F., CAMUS, P.P., LARSON, D.J., HOLZMAN, L.M. & BAJIKAR, S.S. (1996). On the many advantages of local-electrode atom probes. *Ultramicroscopy* 62, pp. 29-42
- KELLY, T.F. & LARSON, D.J. (2000) Local electrode atom probes. *Mater. Char.* 44 (1-2), pp. 59-85
- MULLER, E.W., PANITZ, J.A. & MCCLANE, S.B. (1968). The atom-probe field ion microscope. *Rev. Sci. Instrum.* 39, pp. 83-86
- KINNO, T., AKUTSU, H., TOMITA, M., KAWANAKA, S., SONEHARA, T., HOKAZONO, A., RENAUD, L., MARTIN, I., BENBALAGH, R., SALLE, B & TAKENO, S. (2012). Influence of multi-hit capability on quantitative measurement of NiPtSi thin film with laser-assisted atom probe tomography, *Appl. Sur. Sci.*, 259, pp. 726-730

LARSON, D.J., PROSA, T.J., ULFIG, R.M., GEISER, B.P. & KELLY, T.F. (2013). D.J. Larson, T.J. Prosa, R.M. Ulfig, B.P. Geiser and T.F. Kelly, *Local Electrode Atom Probe Tomography: A User's Guide*, Verlag, New York, USA: Springer

LI, T., BAGOT, P.A.J., MARQUIS, E.A., TSANG, S.C.E & SMITH, G.D.W. (2012). Characterization of Oxidation and Reduction of Pt-Ru and Pt-Rh-Ru Alloys by Atom Probe Tomography and Comparison with Pt-Rh, *J. Phys. Chem. C*, 116(33) pp. 17633-17640

MARCEAU, R.K.W., CHOI, P. & RAABE, D. (2013). Understanding the detection of carbon in austenitic high-Mn steel using atom probe tomography. *Ultramicroscopy*, 132, 239-247

MEISENKOTHEN, F., STEEL, E.B., PROSA, T.J., HENRY, K.T. & PRAKASH KOLLI, R. (2015). Effects of detector dead-time on quantitative analyses involving boron and multi-hit detection events in atom probe tomography, *Ultramicroscopy*, 159, pp. 101-111

MEISNAR, M., MOODY, M.P. & LOZANO-PEREZ, S. (2015). Atom probe tomography of stress corrosion crack tips in SUS316 stainless steels, *Corrosion Science*, 98, pp. 661-671

MOODY, M.P., GAULT, B., STEPHENSON, L.T., MARCEAU, R.K.W., POWLES, R.C., CEGUERRA, A.V., BREEN, A.J. & RINGER, S.P. (2011). Lattice Rectification in Atom Probe Tomography: Toward True Three-Dimensional Atomic Microscopy, *Microscopy and Microanalysis* 17(2), 226-239

PANITZ, J.A. (1973). The 10cm atom probe. *Rev. Sci. Instrum.* 44(8), pp. 1034-1038

PEDRAZZINI, S., CHILD, D.J., WEST, G., DOAK, S.S., HARDY, M.C., MOODY, M.P. & BAGOT, P.A.J. (2016). Oxidation behaviour of a next generation polycrystalline Mn containing Ni-based superalloy, *Scripta Materialia*, 113, pp. 51-54

PROSA, T.J., GEISER, B.P., LAWRENCE, D.J., OLSEN, J.D. & LARSON, D.J. (2014). Developing detection efficiency standards for atom probe tomography. *Proc. SPIE 9173, Instrumentation, Metrology, and Standards for Nanomanufacturing, Optics and Semiconductors VIII*, 917307

ROBERTSON, C., PANIGRAHI, B.K., BALAJI, S., KATARIA, S., SERRUYS, Y., MATHON, M.-H. & SUNDAR, C.S. (2012), Particle Stability in Model ODS Steel irradiated up to 100 dpa at 600°C: TEM and nano-indentation investigation, *J. Nucl. Mat.*, 426, pp. 240-246

ROLANDER, U. & ANDRÉN, H.-O. (1989). Statistical correction for pile-up in the atom-probe detector system. *J.Phys.Colloques.* 50, C-8-529-C8-534

SANTHANAGOPALAN, D., SCHRIEBER, D.K., PEREA, D.E., MARTENS, R.L., JANSSEN, Y., KHALIFAH, P. & MENG, Y.S. (2015). Effects of laser energy and wavelength on the analysis of LiFePO₄ using laser assisted atom probe tomography, *Ultramicroscopy*, 148, pp. 57-66

STEINER, T., MEKA, S.R., RHEINGANS, B., BOSCHOFF, E., WALDENMAIER, T., GUMA, Y., MARTIN, T.L., BAGOT, P.A.J., MOODY, M.P. & MITTEMEIJER, E.J. (2016). Continuous and discontinuous precipitation in Fe-1 at.% Cr-1 at.% Mo alloy upon nitriding; crystal structure and composition of ternary nitrides, *Philosophical Magazine*, 96(15), pp. 1509-1537

STYMAN, P.D., HYDE, J.M., WILFORD, K., MORLEY, A. & SMITH, G.D.W. (2012). Precipitation in long term thermally aged high copper, high nickel model RPV steel welds, *Progress in Nuclear Energy* 57, pp. 86-92

THOMPSON, K., LAWRENCE, D.J., LARSON, D.J., OLSEN, J.D., KELLY, T.F. & GORMAN, B. (2007). In-situ site-specific specimen preparation for atom probe tomography. *Ultramicroscopy* 107, pp.131-139

THUVANDER, M., KVIST, A., JOHNSON, L.J.S, WEIDOW, J. & ANDRÉN, H.-O. (2013). Reduction of multiple hits in atom probe tomography. *Ultramicroscopy*, 132, pp. 81-85

VALLEY, J.W., CAVOSIE, A.J., USHIKUBO, T., REINHARD, D.A., LAWRENCE, D.F., LARSON, D.J., CLIFTON, P.H., KELLY, T.F., WILDE, S.A., MOSER, D.E. & SPICUZZA, M.J. (2014). Hadean age for a post-magma-ocean zircon confirmed by atom-probe tomography, *Nature Geoscience* 7, pp. 219-223

Material	Analysis Mode	Pulse Fraction (voltage mode)	Laser Energy (laser mode)	Temperature	Pulse Frequency
SG RPV Steel	Voltage	20%	N/A	50K	200kHz
ODS Steel	Laser	N/A	Varied	50K	200kHz
M50 Bearing Steel	Laser	N/A	0.4nJ (LEAP 3000) 44pJ (LEAP 5000)	50K	200kHz
Silicon	Laser	N/A	0.4nJ (LEAP 3000) 50pJ (LEAP 5000)	50K	200kHz

Table 1: Summary of APT analysis conditions used for each of the four materials used in this study, for both the LEAP 3000 and LEAP 5000 instruments.

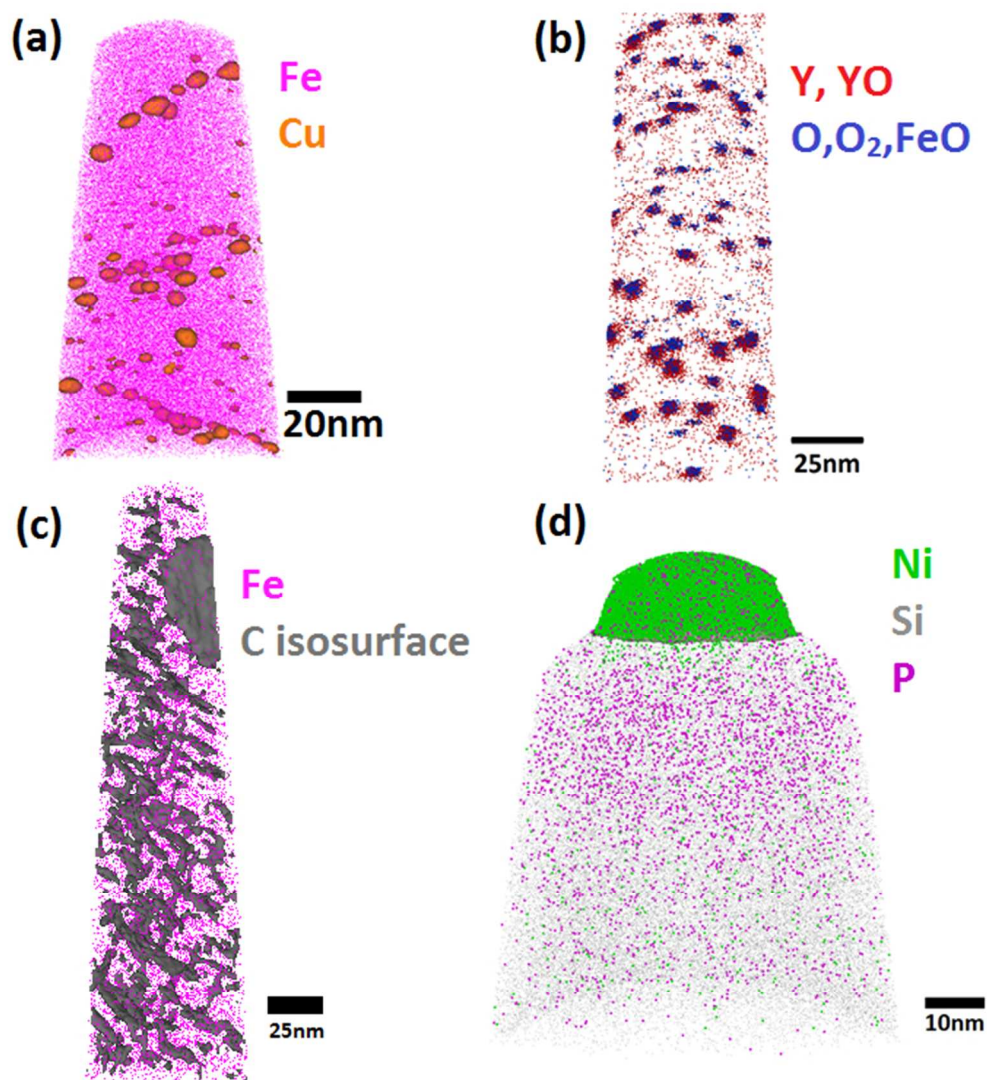


Figure 1: Atom maps for the materials used during this study. (a) Cu clusters in a thermally aged Reactor Pressure Vessel (RPV) steel, (b) Yttrium Oxide clusters in an Oxide Dispersion Strengthened (ODS) steel, (c) carbides in a bearing steel and (d) phosphorus at the surface of implanted silicon. All atom maps shown were analysed using the LEAP 3000.

181x196mm (96 x 96 DPI)

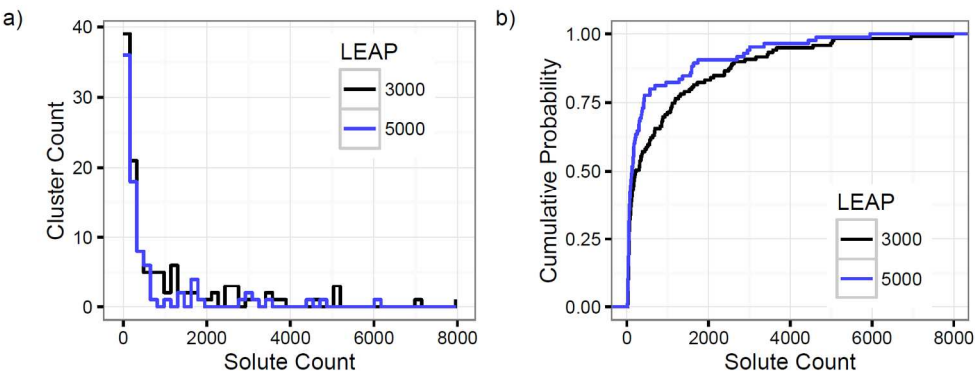


Figure 2: (a) Comparison of the size distribution of Cu clusters in an RPV steel analysed on the LEAP 3000 (black) and LEAP 5000, (blue). (b) Empirical cumulative distribution function comparing the two distributions.

505x196mm (96 x 96 DPI)

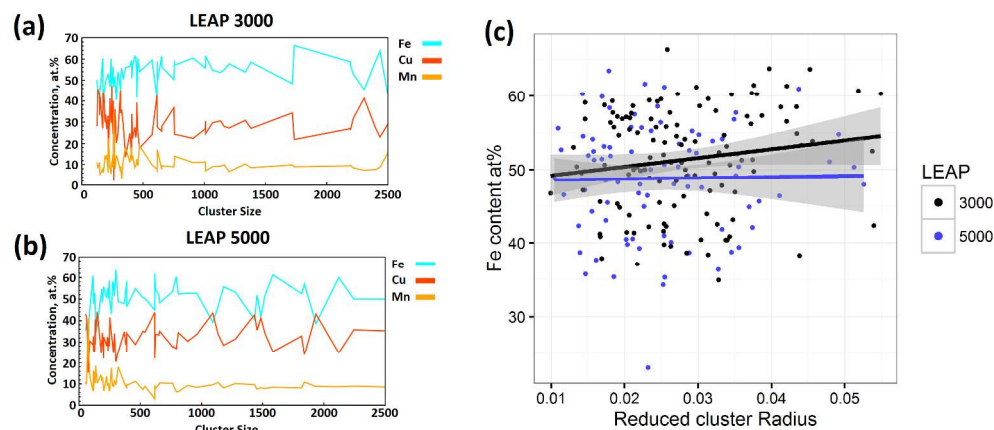


Figure 3: Compositions of the Cu clusters in (a) four LEAP 3000 datasets and (b) five LEAP 5000 datasets, against cluster size, as defined by the number of ranged ions. The Fe content averaged 53 at.% in the LEAP 3000 and 50 at.% in the LEAP 5000. (c) shows the Fe content as a function of cluster radius for the two instruments.

860x371mm (96 x 96 DPI)

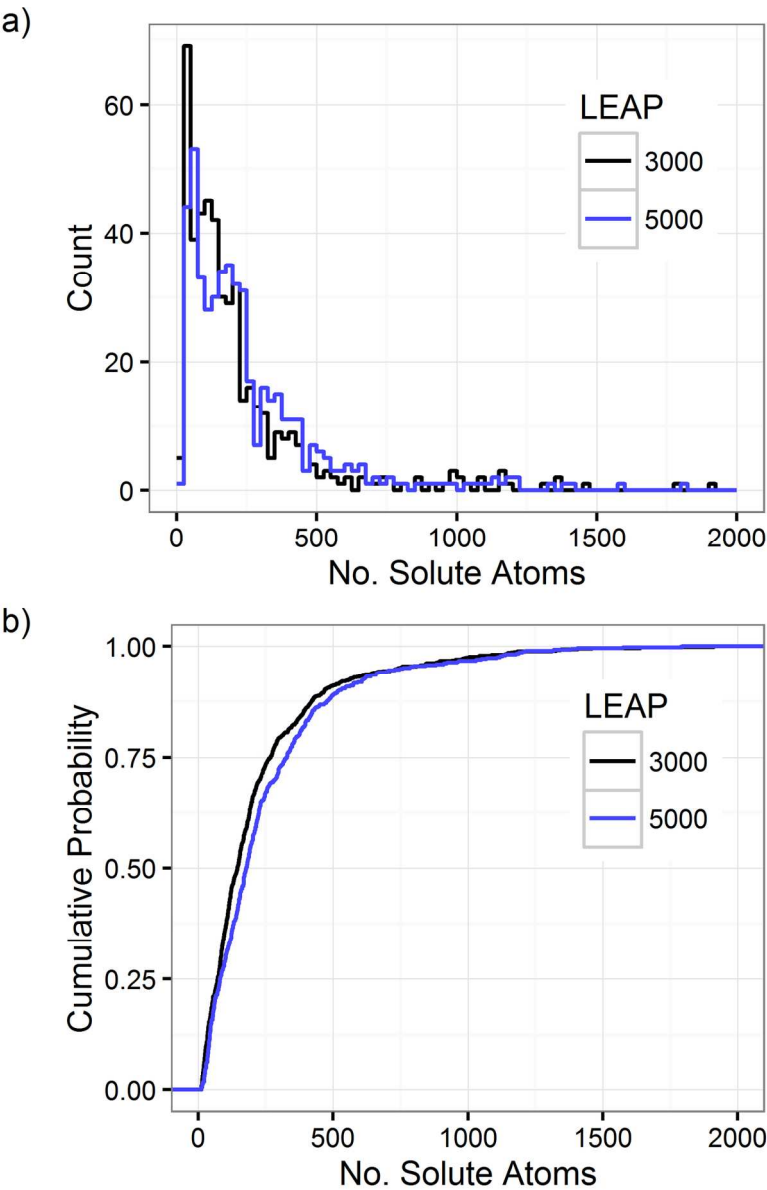


Figure 4: (a) Size distribution of YO particles in an ODS steel analysed using the LEAP 3000 (black) and LEAP 5000 (blue). (b) shows the empirical cumulative distribution function for the same data.

127x192mm (300 x 300 DPI)

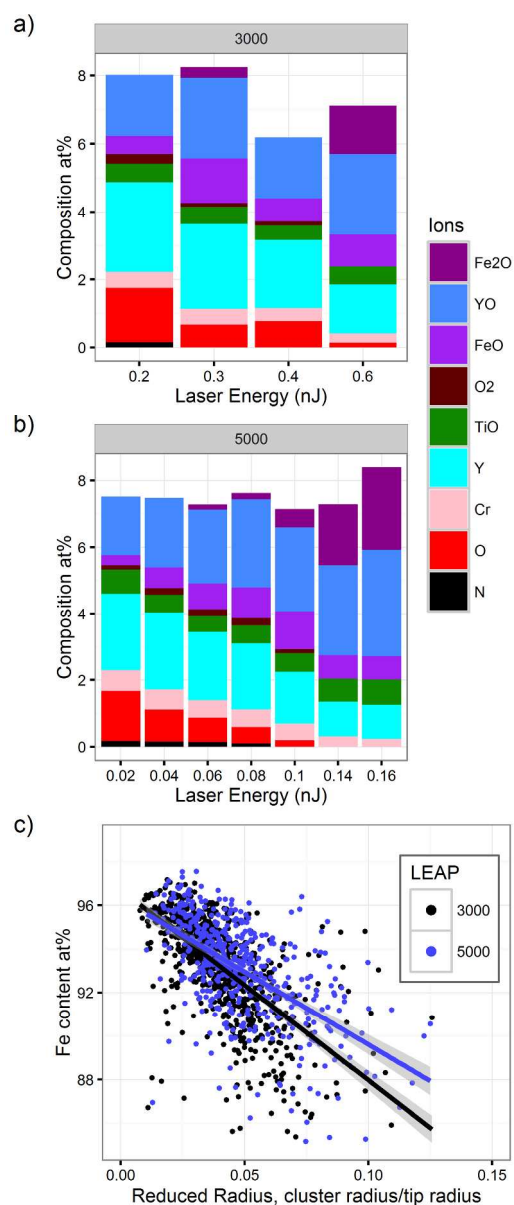


Figure 5: (a) change in YO particle chemistry with increasing laser energy on the LEAP 3000 (b) change in YO particle chemistry with laser energy on the LEAP 5000, (c) the relationship between cluster size and Fe content included from the matrix in the oxide particles, with black representing data from the LEAP 3000 and blue representing data from the LEAP 5000.

177x414mm (300 x 300 DPI)

	LEAP 3000	LEAP 5000
No of carbides	8	8
Average Carbide ion count	170	243
Average carbide volume (nm ³)	36.0 nm ³	36.2 nm ³
Fe at.%	20.0%	27.2%
C at.%	35.2%	26.1%
Cr at.%	19.1%	19.6%
Mo at.%	17.2%	15.9%
Carbide C multiples	74.3%	85.9%

Table 1: Comparison of the size, number density and composition of selected M₂C carbides analysed from a bearing steel in the LEAP 3000 and LEAP 5000 instruments.

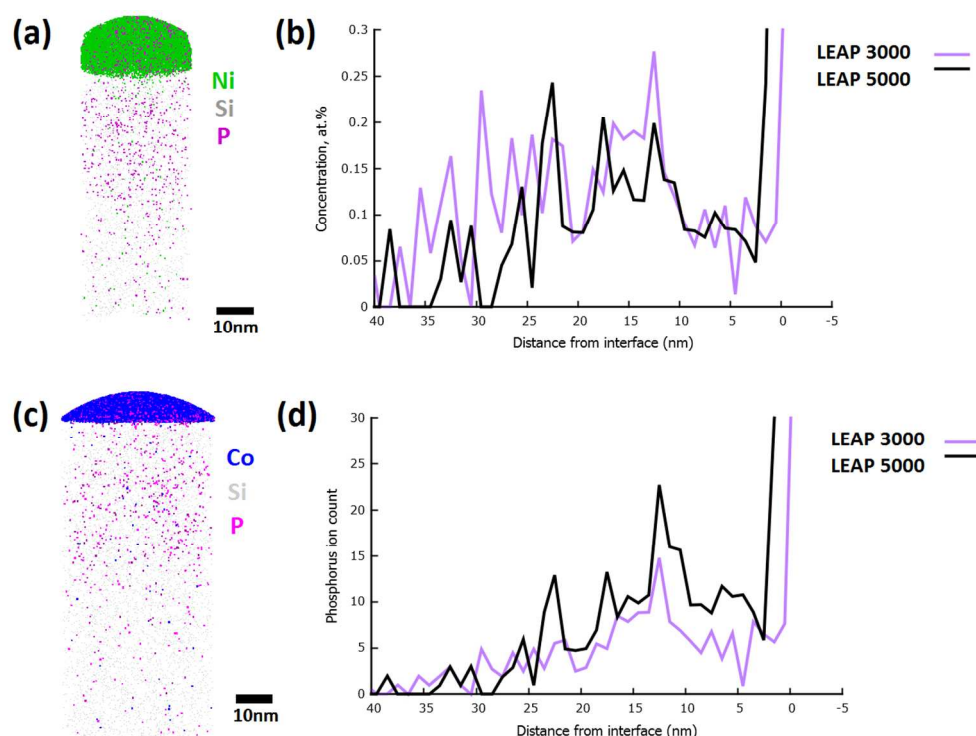


Figure 6: (a) 30x30x100nm region of interest of a phosphorus-implanted silicon sample with nickel cap analysed using the LEAP 3000. (b) Comparison of the phosphorus concentration profile at the surface of both ion-implanted silicon materials. (c) 30x30x100nm region of interest of a phosphorus-implanted silicon sample with cobalt cap analysed using the LEAP 5000. (d) Ion counts of phosphorus across the same region shown in (b).

355x265mm (96 x 96 DPI)